

## Surface Reduction Study of Monoazo Dyes by Adsorptive Square Wave Voltammetry

Gang Xu,\* John J. O'Dea & Janet G. Osteryoung<sup>†</sup>

Department of Chemistry, North Carolina State University, Raleigh, NC 27695-8204, USA

(Received 7 June 1995; accepted 10 August 1995)

### ABSTRACT

*The surface reduction behavior of nine monoazo dyes at the static mercury drop electrode has been studied by adsorptive square wave voltammetry. Three types of surface reduction behavior are seen among the nine azo dyes. Two of them are modeled as a two-step mechanism in which the first step is a quasi-reversible reduction followed by a totally irreversible reduction. For those dyes having strong electron-donating groups such as amino or dimethylamino, the second reduction occurs at a potential almost the same as that of the first, and only one peak is observed. The second step gradually separates from the first step as the pH-value of the solution increases. For those azo dyes having methoxy or hydroxy substituents, two peaks are observed; one is quasi-reversible, the other is totally irreversible. The second, irreversible step gradually overlaps the first step as the pH-value of the solution decreases. The third type voltammogram of these monoazo dyes displays a single irreversible peak that is modeled as a four-electron one-step irreversible reduction. These surface reduction behaviors are quantitatively explained by the proposed models. Kinetic parameters for these surface reactions are obtained by non-linear least squares (COOL) analysis of the voltammograms. These techniques are useful both for establishing mechanisms and chemical analysis.*

### INTRODUCTION

Azo compounds are the oldest and largest class of industrial, synthesized organic dyes and are usually considered the class with the fullest shade

\*Permanent address: Department of Applied Chemistry, Jiangsu Institute of Petrochemical Technology, Changzhou, Jiangsu 213016, People's Republic of China.

<sup>†</sup>Corresponding author.

range and most diverse uses. There are more than three thousand azo dyes currently in use all over the world. The great majority of them are monoazo compounds, which have the common structure unit of the azo chromophore,  $\text{—N=N—}$ , linking two aromatic systems. The textile industry is the largest consumer of dyestuffs, and it is estimated that 10–15% of the dye is lost during the dyeing process and is released as effluent.<sup>1</sup> Some azo dyes<sup>2–4</sup> have been reported to be toxic or carcinogenic.

Five of the nine synthetic colorants now permitted in food in the United States are monoazo dyes.<sup>5,6</sup> By properly blending the nine colorants, nearly any shade can be produced. Dozens of additional monoazo dyes are permitted in drugs and cosmetics.<sup>6</sup> Thus much attention has been focused on the biological activity and metabolism of the dyes *in vivo*.

Various workers<sup>7–17</sup> have investigated the biodegradation of azo dyes by bacteria. They have reported that some anaerobic bacteria, including some common components of mammalian intestinal microflora and microorganisms found in the mud of lakes and slow-moving rivers, are able to reduce some azo dyes under anaerobic conditions. The gastrointestinal tract, particularly the colon, is the most anaerobic environment in the body. Generally, the metabolites are the corresponding amines, which shows that biodegradation involves cleavage of the azo linkage. For instance, a bacterium identified as a *Proteus* species, isolated by Roxon *et al.* from rat large intestine, was shown to reduce tartrazine (CI Acid Yellow 23) anaerobically under oxygen-free nitrogen.<sup>8</sup> Nearly all human subjects carry *Proteus*.<sup>8</sup> Anaerobes identified as *Eubacterium hadrum*, *Clostridium clostridioforme*, and others isolated by Rafii<sup>12</sup> from human feces, are capable of reducing CI Direct Blue 15 anaerobically (5%  $\text{CO}_2$ , 10% hydrogen, 85% nitrogen). Biodegradability depends mainly on chemical structures.<sup>15,16</sup> Some authors have noted that, prior to reduction, molecules of azo dyes must be transported to and adsorb onto the cell membrane of bacteria. There is a continuing need for investigation into the metabolism and carcinogenic properties of azo dyes to provide a basis for the confident prediction of their biological activity from their chemical structures.<sup>13</sup>

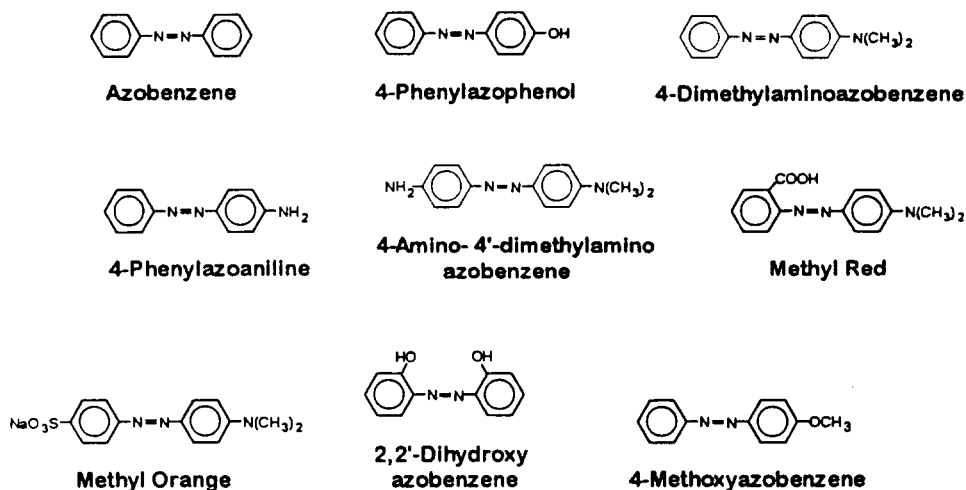
Azo compounds are capable of adsorbing on mercury surfaces. The conditions employed in adsorptive stripping voltammetry are very similar to the above-mentioned conditions in biodegradation. Therefore, a study of the surface electrochemical reduction mechanism of azo compounds may give useful information about metabolic reactions of these compounds in biological systems. Furthermore, the electrochemical kinetics and energetics yield information about energy levels and may be useful for predicting photochemical reactivity. Finally, the electrochemical methods are simple, fast, and inexpensive and can be used for chemical analysis.

The polarographic behavior of azo dyes has been studied extensively.<sup>18–24</sup>

A disproportionation mechanism has been proposed to explain the homogeneous reduction of azo compounds in aqueous solutions. Boto and Thomas,<sup>25</sup> and Kastening<sup>26</sup> have investigated the adsorption of Methyl Red, and Methyl Orange and 4-aminoazobenzene, respectively, on the dropping mercury electrode. Laviron and Mugnier have studied the surface and volume electroreduction of azobenzene by linear sweep voltammetry.<sup>27</sup> Adsorptive preconcentration of 4-aminoazobenzene has been used in a fast scan differential pulse voltammetry determination scheme.<sup>28</sup> However, little information about the kinetic studies of azo compounds by pulse voltammetry can be found in the literature.

Square wave voltammetry<sup>29,30</sup> combined with adsorptive accumulation has proven to be one of the most sensitive analytical techniques for ultra-trace determination of azo compounds.<sup>31</sup> The present work demonstrates that the combination of square wave voltammetry and the COOL algorithm<sup>32-34</sup> allows us to discriminate among various mechanisms for surface reduction of monoazo compounds. The kinetic results in turn allow us to extend conclusions regarding the determination of azobenzene<sup>31</sup> to a variety of azobenzene derivatives.

In this work nine monoazo dyes have been studied by adsorptive square wave voltammetry.



## EXPERIMENTAL

Water was purified by a Millipore Milli-Q purification system. All dyes studied were from Aldrich or Fluka. The dyes of purity > 99% were used as received; otherwise, recrystallization was repeated three times from 95% ethanol. The free acid form of Methyl Red (Aldrich) was purified by

Soxhlet extraction with toluene and recrystallized three times. All other reagents were ACS reagent grade.

Supporting electrolytes were 0.1 M acetate buffer or 0.1 M Britton–Robinson buffer adjusted with 2 M NaOH.

Square wave voltammetry was carried out using an EG&G PARC model 303A static mercury drop electrode for the working electrode. The drop area was 0.0158 cm<sup>2</sup> (medium drop size). All potentials were measured versus a saturated calomel electrode. A platinum wire served as the counter electrode. The potentiostat used was an EG&G PARC 273 remotely controlled by a personal computer (486/33 MHz). The software employed for both experimental control and data analysis is functionally equivalent to the EG&G PARC 270 software. The 486 computer was also used for data analysis.

Adsorptive square wave voltammetry consists of two steps as shown in Fig. 1. First, the electrode is held at a conditioning potential,  $E_c$ , for a period of conditioning time,  $t_c$ . The conditioning potential is chosen such that the analyte adsorbs onto the electrode surface without reaction. The solution near the electrode surface is depleted during the conditioning time, so that diffusive contributions of reactant during the relatively short stripping step are negligible. The stripping step consists of scanning the potential from an initial value,  $E_i$ , to a final value,  $E_f$ , with square wave modulation. The waveform is a square wave of frequency  $f = 1/(2t_p)$  and amplitude  $E_{sw}$  superimposed on a staircase of step height of  $\Delta E_s$ . The quantity  $t_p$  is the characteristic pulse width of the waveform. Currents are sampled at the end of pulses as indicated by the numbered small circles. A net current voltammogram is obtained by subtracting the even-numbered reverse current from the corresponding odd-numbered forward current and plotting the net result versus the base staircase potential. In this work,  $E_i$  is coincident with  $E_c$ , that is, the stripping sequence begins from the conditioning potential. Step height,  $\Delta E_s$ , and amplitude,  $E_{sw}$ , used were 5 and 25 mV, respectively.

Unless otherwise noted, all the stock solutions were millimolar concentration and prepared by dissolving an appropriate amount of dye in 10 M acetic acid. For Methyl Red and 2,2'-dihydroxyazobenzene, stock solutions were prepared by dissolving the dye in a minimum amount of 0.1 M sodium hydroxide, then diluting to volume with water. The stock solutions were stored in darkness. Working solutions were prepared daily from the stock solutions. Solutions were deoxygenated and blanketed with presaturated argon before analysis. All experiments were conducted at a room temperature of  $22 \pm 0.2^\circ\text{C}$ . All voltammograms are the average of three successive scans, each recorded with a new mercury drop. Blanks were obtained by recording voltammograms of the appropriate buffer solutions under the same conditions as for the sample solutions.

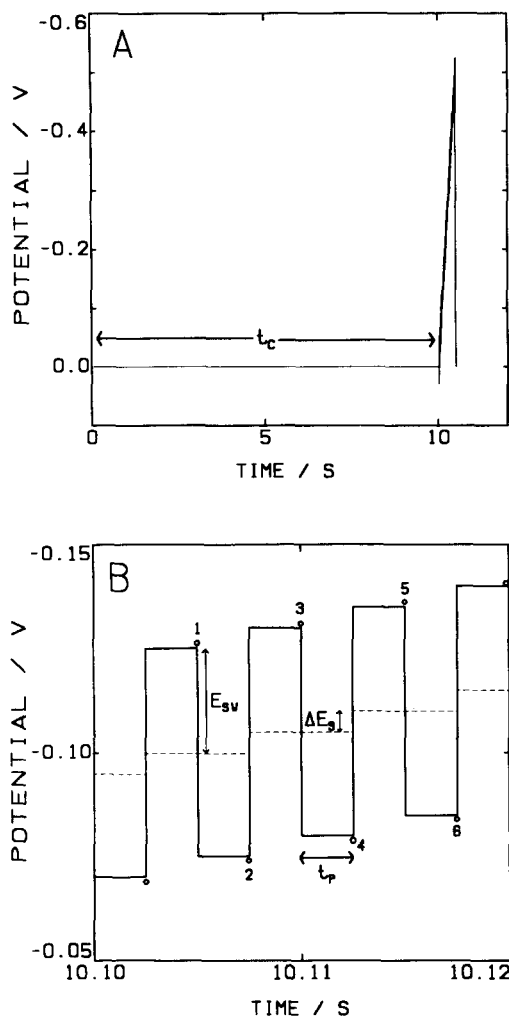


Fig. 1. Square wave adsorptive stripping: (A) preconcentration step; (B) waveform.

Controlled-potential coulometry was performed by using an EG&G PARC 173 potentiostat equipped with a model 197 digital coulometer. A two-compartment cell was used with a mercury pool working electrode, a saturated calomel reference electrode, and a platinum-foil counter electrode. The counter electrode was placed in a separate compartment containing 0.1 M pH buffer and isolated from the working electrode compartment by a sintered glass disk. The sample solution was 5.00 ml of 10  $\mu$ M dye in 0.1 M pH buffer. The electrolysis was carried out at the appropriate potential for at least 40 minutes, until the color of the catholyte was discharged.

All pH measurements were made using a Corning Model 220 pH Meter with a combined glass and Ag/AgCl electrode.

## RESULTS AND DISCUSSION

### Adsorptive behavior

Figure 2 displays net peak currents obtained for 2  $\mu\text{M}$  4-phenylazophenol. Peak heights increase with increasing conditioning time,  $t_c$ , and currents quickly return to zero as the peak potentials are passed. These features are consistent with reduction of adsorbate and were observed for the other dyes studied.

Figure 3 shows a plot of net peak current,  $I_p$ , of Methyl Red against  $C^*t_a^{1/2}$ , where  $C^*$  is the bulk concentration and  $t_a$  is the accumulation time. Accumulation time is the time elapsed from the formation of the mercury drop to the time that the current reaches its maximal value. This plot illustrates that the adsorption of Methyl Red on the mercury surface is diffusion-controlled and that the maximal coverage is a monolayer. For diffusion-controlled adsorption at a planar electrode, the relationship between the surface concentration,  $\Gamma$ , and the accumulation time,  $t_a$ , is given by eqn (1)

$$\Gamma = 2C^* \sqrt{\frac{Dt_a}{\pi}}, \quad (1)$$

in which  $D$  is the diffusion coefficient of the reactant. For the experimental conditions employed here, planar diffusion is closely approximated for the

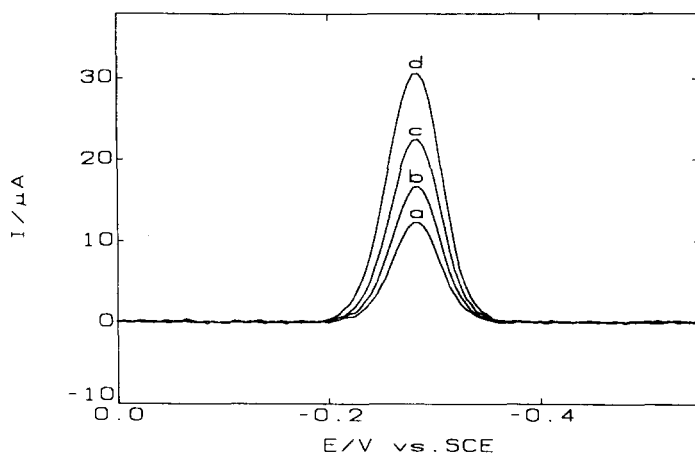


Fig. 2. Dependence of net current on conditioning time,  $t_c$ : 2  $\mu\text{M}$  4-phenylazophenol, 0.1 M acetate buffer, pH 4.6,  $f = 200$  Hz,  $t_d/s$  = (a) 5, (b) 10, (c) 20, (d) 40.

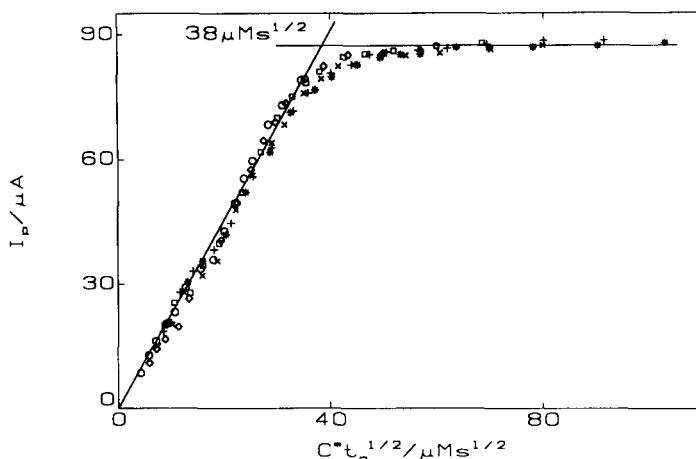


Fig. 3. Net peak current versus  $C^*t_a^{1/2}$ : 4–9  $\mu\text{M}$  Methyl Red in 0.1 M acetate buffer at pH 4.6,  $f = 350$  Hz.  $C^*/\mu\text{M} = (\bigcirc)$  4,  $(\diamond)$  5,  $(\square)$  6,  $(\times)$  7,  $(+)$  8,  $(*)$  9.

spherical electrode. For Methyl Red, the value of  $D$  is estimated to be  $5.6 \times 10^{-6} \text{ cm}^2 \text{ s}^{-1}$  by the Stokes-Einstein equation:<sup>35</sup>  $D = K/(V_m)^{1/3}$ . In this equation, the value of  $K$  for an aqueous solution at  $25^\circ\text{C}$  is  $3.31 \times 10^{-5} \text{ cm s}^{-1}$  and  $V_m$  is the molecular mass (269.3) divided by density ( $1.32 \text{ g cm}^{-3}$ ).<sup>36</sup> An average area of  $1.6 \text{ nm}^2$  per molecule on the surface can be calculated from the maximal coverage. This compares reasonably well with a value of  $1.7 \text{ nm}^2$  calculated for a flat orientation by applying the method of Soriaga *et al.*<sup>37</sup> to the crystallographic data of Moreiras and Solans.<sup>36</sup>

Figure 3 indicates that the maximal net peak current density for analytical purposes is about  $5500 \mu\text{A cm}^{-2}$  at 350 Hz.

### Surface reduction behavior

Figure 4 compares voltammograms of azobenzene and Methyl Red at  $10 \mu\text{M}$  concentration in 0.1 M acetate buffer at pH 4.6. Figure 4A shows a small broad peak at  $-1.1 \text{ V}$  corresponding to the reduction of hydrazobenzene to aniline. Constant potential coulometry of azobenzene at  $-0.35 \text{ V}$  indicates that two electrons are consumed per molecule. However, constant potential coulometry at  $-1.2 \text{ V}$  shows that a total of four electrons are consumed per molecule. Apparently the partially reduced form, hydrazobenzene, is a stable intermediate at potentials less than  $-1.0 \text{ V}$ . In the case of Methyl Red, however, just one peak is observed, as shown in Fig. 4B. The number of electrons transferred per molecule measured by constant potential coulometry at  $-0.35 \text{ V}$  is four. This behavior can be explained by the four-electron two-step reduction model shown in reaction sequence (2).

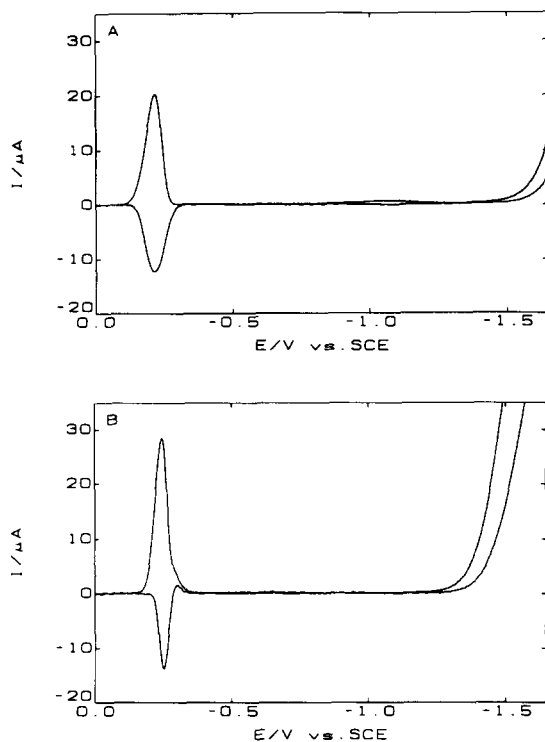
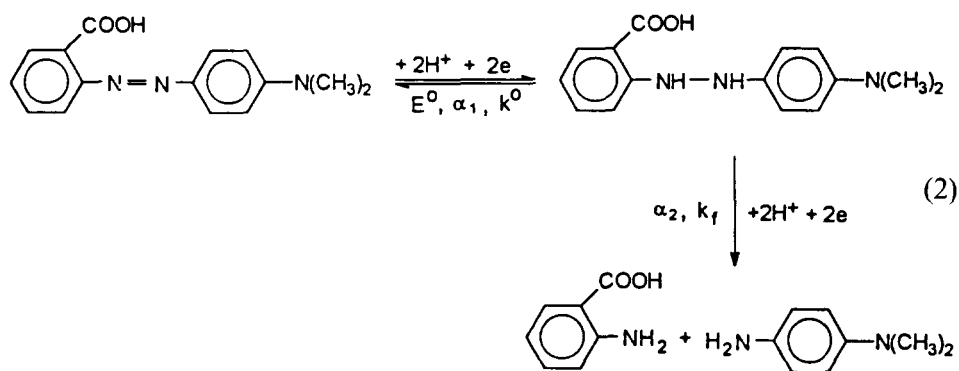


**Fig. 4.** Voltammograms of 10  $\mu\text{M}$  azobenzene (A) and Methyl Red (B) in 0.1 M acetate buffer, pH 4.6,  $f = 300$  Hz,  $t_c = 5$  s. Upper curves: forward currents; lower curves: reverse currents.



The first step is a two-electron quasi-reversible reduction yielding the hydrazo form, as in the case of azobenzene. The hydrazo form then undergoes irreversible reductive-cleavage to give the corresponding aromatic amines. On the voltammetric time scale the azo/hydrazo moiety can 'turn over' several times, following the waveform through reducing and oxidizing potentials. A relatively strong differential signal is developed under these



circumstances. Eventually the second step, irreversible cleavage to amines, destroys the electroactivity of the first step, leading to an overall four-electron irreversible reduction. In Methyl Red the dimethylamino substituent increases the basicity of the azo group over that for azobenzene. This facilitates protonation of the azo group and subsequent cleavage of the N—N bond. The reduction potential of the second process shifts to more positive values and overlaps the first process. The relative rates of the two processes control the shape of the resulting voltammogram.

The voltammogram of Fig. 4B is shown together with the best-fitting theoretical curve in Fig. 5A. The circles are experimental data, and the solid line is the calculated current for the four-electron, two-step mechanism. The best-fitting curve is obtained by the COOL algorithm, in which the experimental current is presumed to be a linear function of the dimensionless model current,  $\psi$ .<sup>31</sup>

$$i = a\psi + b, \quad (3)$$

where  $a$  is the slope and  $b$  is the intercept. The function  $\psi$ , defined as

$$\psi = i[nFA\Gamma/t_p] \quad (4)$$

depends on the potential sequence, temperature and reduction model. Here  $A$  is the area of the mercury electrode. The fitting procedure is based on a non-linear optimization of the kinetic parameters of the electrode processes, which minimizes the complement of the correlation coefficient,  $(1-R)$ , for the linear regression of the measured current on the theoretical current calculated from the kinetic parameters. The observed shapes of the forward and reverse currents are well described by the model. These shapes are better understood by examination of the current contributions of the individual reaction steps.

Figure 5B shows the theoretical currents for the first and second reaction steps and the total current for the overall process. Note the asymmetry of the forward and reverse currents for the first step, in spite of the fact that the transfer coefficient for the first step is nearly 0.5. Reverse current contributions from the first step are attenuated as electroactivity is destroyed by the second step. The current contributions of the second step are relatively small even though this step contributes one half of the total charge passed. This is a consequence of irreversible kinetics and the small transfer coefficient associated with the second step. Note also the appearance of a small 'tail' on the peak due to the second step. The 'tail' is manifest even though there is no diffusive contribution of electroactive material from bulk solution. It simply reflects a relatively slow irreversible degradation of surface electroactivity.

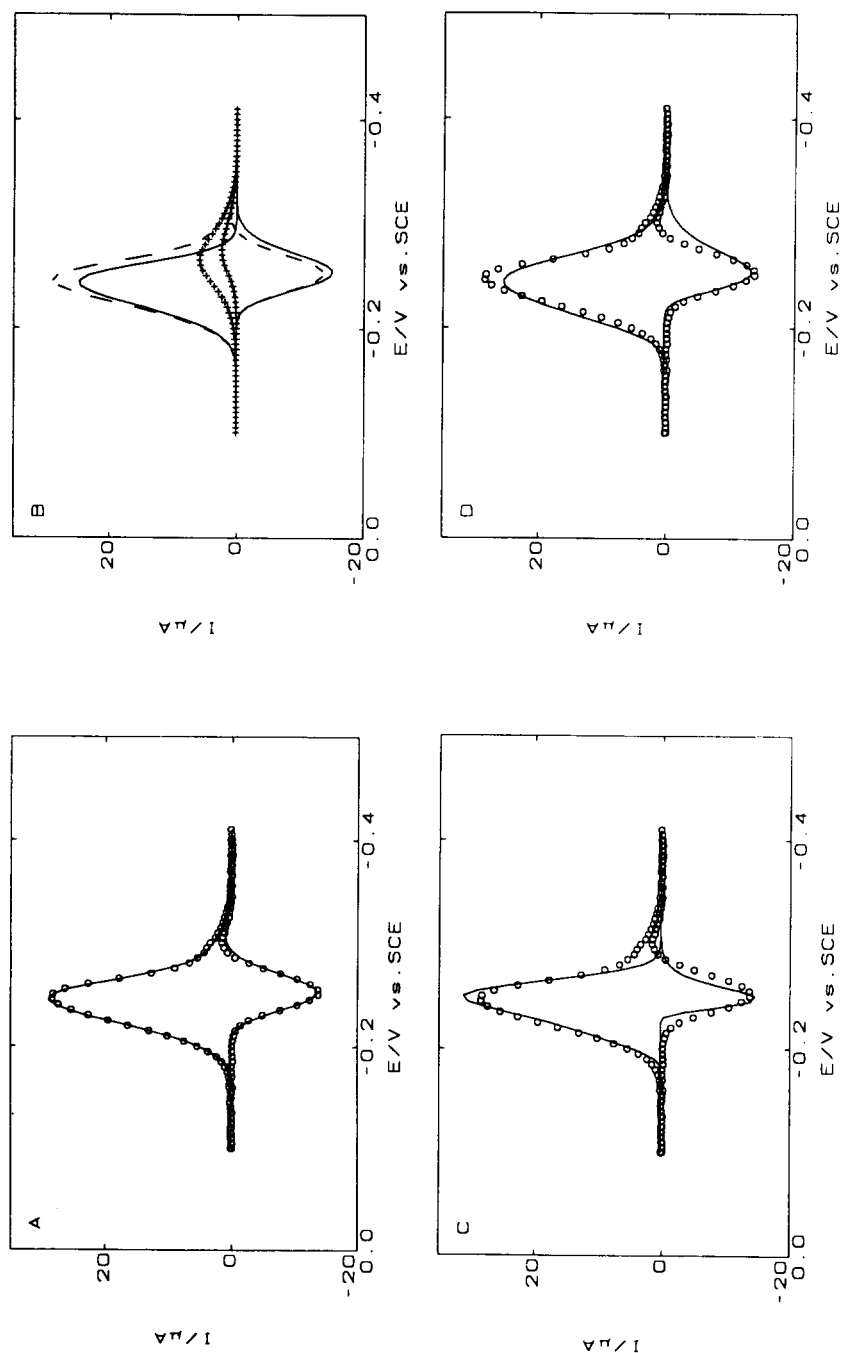
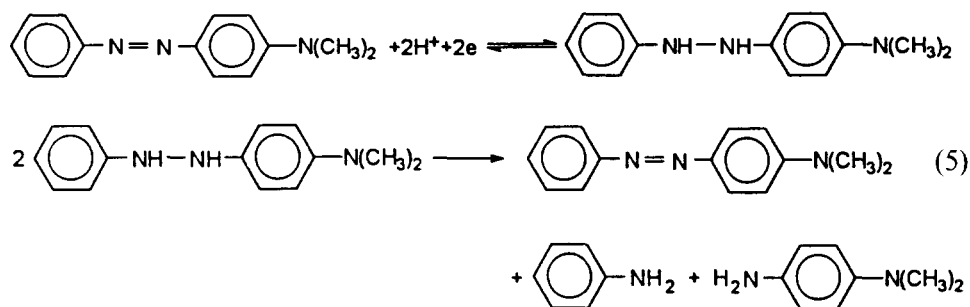


**Fig. 5.** Observed and best fit calculated voltammograms of Fig. 4B. (A) (○) Experimental, (—) calculated for reaction scheme 2.  $R = 0.9993$ ;  $s_y = 0.28 \mu\text{A}$ ;  $s/s_y = 149$ . (B) Calculated partial currents: (---) total, (—) first step, (+) second step. (C) (○) Experimental, (—) calculated for the four-electron one-step quasi-reversible reduction mechanism. (D) (○) Experimental, (—) calculated for a two-electron quasi-reversible reduction mechanism.

The quality of the fit is described by three parameters: the linear regression coefficient,  $R$ , for the plot of observed current vs. model current, the root mean square deviation of the observed current from the model current,  $s_y$ , and the ratio of model current span,  $s$ , to  $s_y$ ,  $s/s_y$ . For this example,  $R = 0.9993$  and  $s_y = 0.28 \mu\text{A}$  for 126 samples, and  $s/s_y = 149$ . For all remaining voltammograms analyzed using COOL, except for those otherwise indicated, the values of these three parameters are given in the corresponding figure captions and tables.

Laitinen and Kneip<sup>18</sup> have investigated the electrochemical behavior of 4-dimethylaminoazobenzene by polarography. They found that in acidic media the polarographic wave height corresponds to a four-electron reduction, whereas above pH 9 the wave height corresponds to a two-electron reduction. However, controlled-potential coulometry showed that four electrons were consumed in both acidic and alkaline media. To explain this anomalous behavior, they proposed the disproportionation mechanism shown in reaction sequence (5).



The unstable hydrazo intermediate undergoes disproportionation, yielding one mole each of the original azo compound and corresponding amines. The regenerated azo compound is then available for further reduction. The rate of disproportionation depends on hydrogen ion concentration. In acidic media, the disproportionation rate is fast in comparison to the lifetime of a mercury drop, so a four-electron polarographic wave is observed. The overall process appears to be a four-electron one-step quasi-reversible reaction. Above pH 9, the disproportionation rate is so slow compared to the polarographic drop lifetime that the disproportionation reaction is negligible, and the polarographic wave height corresponds to a two-electron quasi-reversible reduction. However, the rate is still fast compared to the duration of a coulometric experiment, so coulometry indicates four electrons consumed per molecule. Florence<sup>20</sup> developed this hypothesis further by proposing an acid-catalysed disproportionation mechanism. Later, many investigators<sup>19-24,27</sup> applied disproportionation or acid-catalysed disproportionation mechanisms to explain the electrochemical behavior of azo dyes.

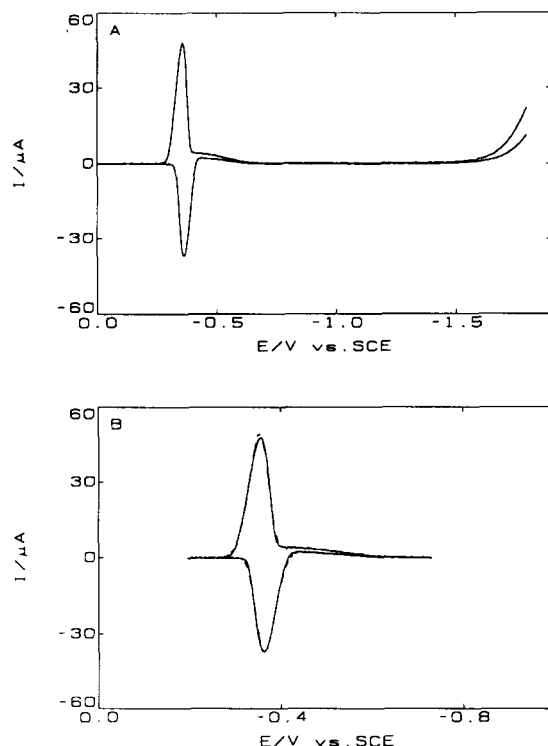


**Fig. 6.** (A) Voltammogram of 10  $\mu\text{M}$  Methyl Red in 0.1 M Britton–Robinson buffer, pH 6.7;  $f = 300$  Hz,  $t_c = 10$  s. (B): Observed and calculated voltammograms of (A), (—) experimental, (---) calculated for reaction scheme 2,  $R = 0.9990$ ;  $s_y = 0.58$   $\mu\text{A}$ ;  $s/s_y = 149$ .

All of this work is at rather high concentration ( $> 0.1$  mM) and presumes that the regenerative disproportionation reaction occurs in the bulk volume of the solution rather at the surface of the electrode.

For the surface reduction of the azo compounds we have studied here, the disproportionation model does not seem to be reasonable. Figure 5C illustrates that the four-electron one-step quasi-reversible reduction mechanism does not fit the experimental data for Methyl Red. Figure 5D indicates that the voltammetric peak is not produced by a two-electron quasi-reversible reduction either.

Since hydronium ions are consumed in the reduction of Methyl Red, the irreversible second step should gradually separate from the first step with increasing the pH value of the solution. A voltammogram of Methyl Red in 0.1 M Britton–Robinson buffer at pH 6.7 is shown in Fig. 6A, which shows that the second step is partially separated from the first step. Figure 6B shows that the two-step model fits the observed voltammogram well. Figure 7A presents a voltammogram of Methyl Red in 0.1 M Britton–Robinson buffer at pH 9.1, which shows that the second step is completely separated

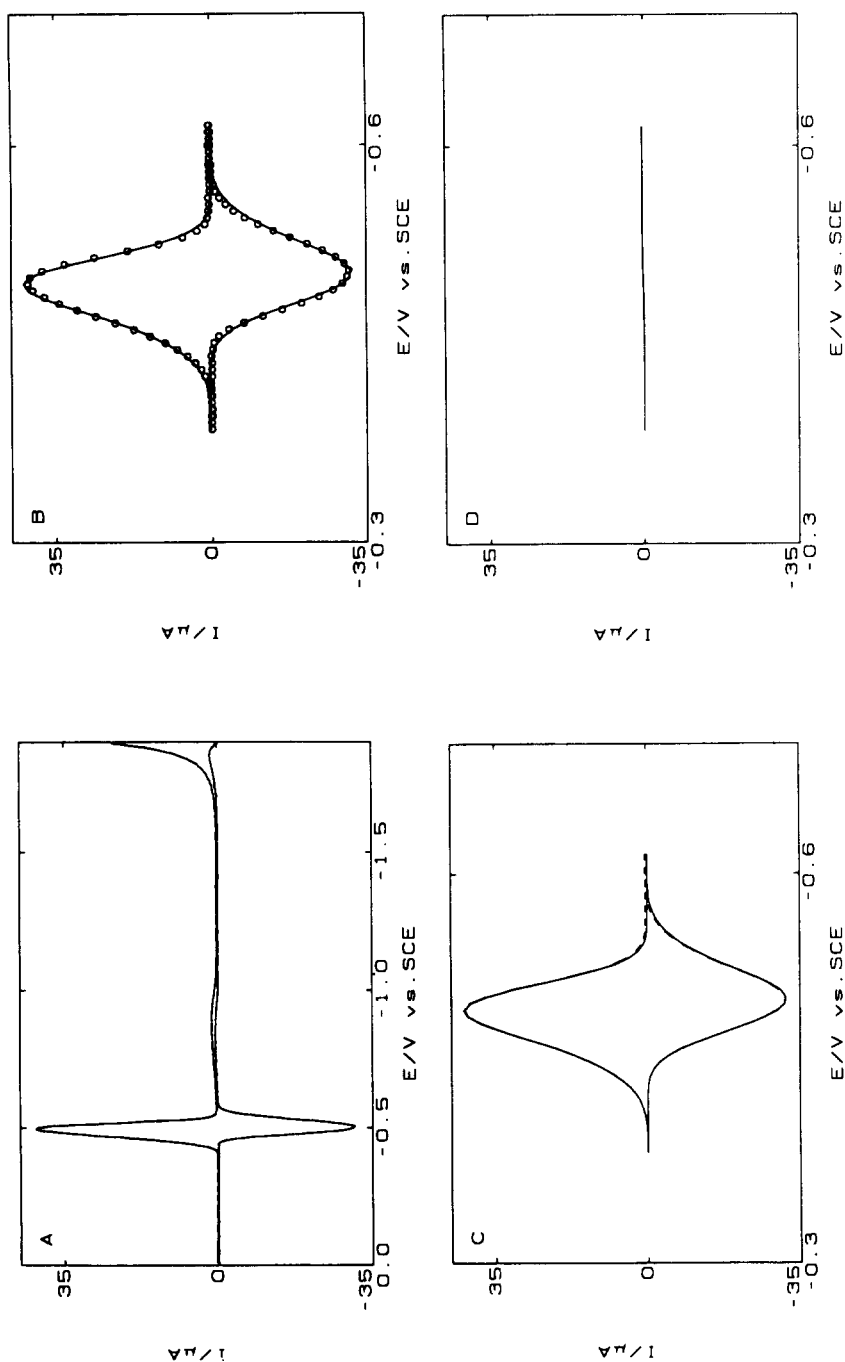


Fig. 7. (A) Voltammogram of 5  $\mu\text{M}$  Methyl Red in 0.1 M Britton-Robinson buffer, pH 9.1;  $f = 350$  Hz,  $t_c = 10$  s. (B) Observed and calculated voltammograms of the first peak in (A), (O) experimental, (—) calculated for a two-electron quasi-reversible reduction model,  $R = 0.9992$ ,  $s_y = 0.34$   $\mu\text{A}$ ,  $s/s_y = 220$ . (C) Calculated currents for a four-electron two-step quasi-reversible reduction model, (—) total, (---) first step. (D) Calculated second step current.

**TABLE 1**  
COOL Analysis of Methyl Red<sup>a</sup>

pH	$E^0/(V \text{ vs } SCE)$	$\alpha_1$	$k^0(s^{-1})$	$\alpha_2$	$k_f(s^{-1})$	$R$	$s_y (\mu A)$	$s/s_y$
4.6	-0.251	0.49	225	0.12	42.2	0.9993	0.28	149
6.7	-0.359	0.50	200	0.12	7.1	0.9990	0.58	149
9.1	-0.495	0.50	158	0.08	1.1	0.9992	0.34	220

<sup>a</sup>See eqn (2).

from the first step, as in the case of azobenzene. Note that the 'tail' almost disappears. The two-electron quasi-reversible surface reduction mechanism describes the first peak very well, as shown in Fig. 7B. Although the two-step model also fits the first peak, the total current is exactly the same as the first step current (Fig. 7C), and the second step current is zero (Fig. 7D). At pH 2.9, the difference between the reduction potentials of Methyl Red for the two steps is even smaller than it is at pH 4.6.

In the two-step reduction model, reaction sequence (2), the kinetic and thermodynamic information contained in the shapes of voltammograms is characterized by five non-linear parameters. These are:  $E^0$ , the standard potential of the first reaction;  $\alpha_1$ , the charge transfer coefficient for the first reaction;  $k^0$ , the standard rate constant for the first reaction;  $\alpha_2$ , the charge transfer coefficient for the second reaction; and  $k_f$ , the forward rate constant for the second reaction referenced to  $E^0$ . Using calculated dimensionless current functions, the COOL algorithm quickly extracts these non-linear parameters from experimental data. The values of the five parameters extracted from the voltammograms of Methyl Red at three different pH values are given in Table 1. The forward rate constant for the second step referenced to  $E^0$  decreases rapidly with increasing pH, because the second irreversible peak shifts negatively faster than the first quasi-reversible peak does as the pH value of the solution increases.

In addition, the slope,  $a$ , of eqn (3) can be obtained from experimental data with the aid of COOL. For the surface reaction, the slope,  $a$ , is given by eqn (4) as  $a = nFA\Gamma/t_p$ . By combining eqns (4) and (1), a value of  $D$  can be calculated. The mean  $D$  value obtained from analysis of 19 voltammograms is  $5.5 \pm 0.5 \times 10^{-6} \text{ cm}^2 \text{ s}^{-1}$ , which agrees well with  $5.6 \times 10^{-6} \text{ cm}^2 \text{ s}^{-1}$  calculated from the Stokes-Einstein equation. The 19 voltammograms are within the linear region of the plot in Fig. 3, corresponding to surface coverage from 35 to 76%. A typical comparison of observed and predicted voltammograms is given in Fig. 8. Either the slope or the value of  $D$  determined therefrom can be viewed as the calibration factor that links peak current to solution concentration.

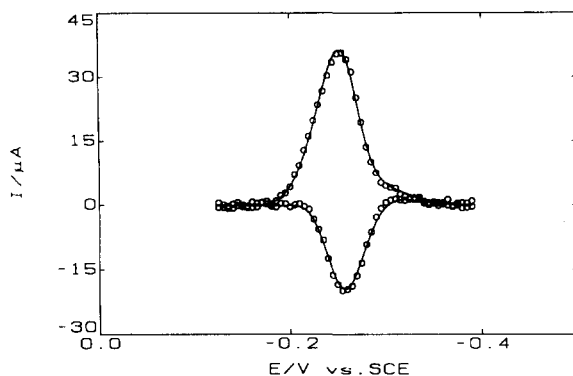
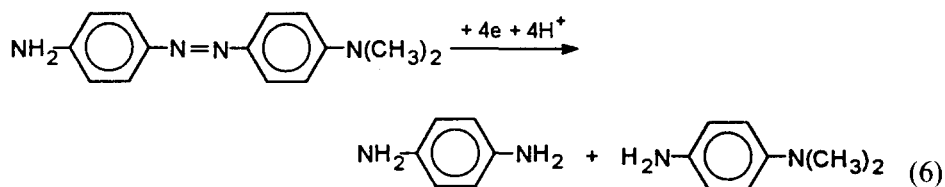


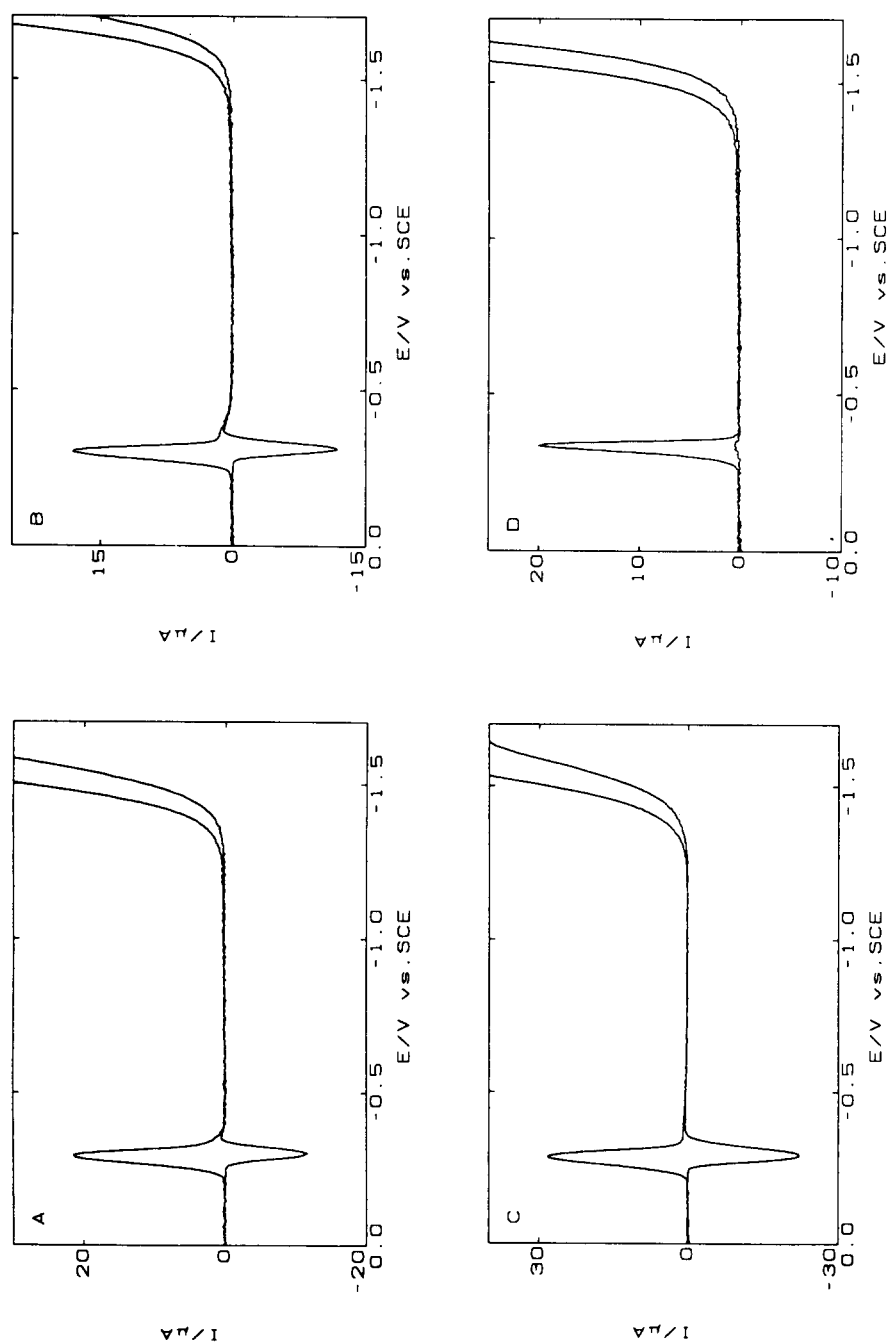
Fig. 8. Observed and calculated voltammograms of 8  $\mu\text{M}$  Methyl Red in 0.1 M acetate buffer, pH 4.6,  $f = 350$  Hz,  $t_c = 10$  s, surface coverage 67%. (○) Experimental, (—) calculated for reaction scheme 2;  $a = 293$   $\mu\text{A}$ ,  $b = 0.1$   $\mu\text{A}$ ,  $D$ -value obtained is  $5.48 \times 10^{-6}$   $\text{cm}^2 \text{s}^{-1}$ .  $R = 0.9990$ ;  $s_y = 0.57$   $\mu\text{A}$ ;  $s/s_y = 98$ .

Figure 9 shows voltammograms of four more monoazo dyes having a dimethylamino or amino substituent para to the azo group. The first three voltammograms are of the Methyl Red type. The two-step model describes the observed peaks very well. Two examples of the good agreement between the data and the model are given in Fig. 10.

The location of *para* and *para'* electron-donating groups, dimethylamino and amino, in the azo dye 4-amino-4'-dimethylaminoazobenzene is so favorable to protonation of the hydrazo intermediate and cleavage of the  $-\text{N}-\text{N}-$  bond that the voltammetric peak is totally irreversible, as shown in Fig. 9D. The overall process is a four-electron one-step irreversible reduction (eqn (6)). Figure 11 demonstrates that the theoretical curve for the four-electron one-step irreversible surface reduction model describes the observed voltammogram.



The kinetic and thermodynamic parameters for the four-electron two-step mechanism extracted from voltammograms of the four dyes having an amino or dimethylamino substituent are listed in Table 2. The  $k_f$  value for 4-phenylazoaniline is less than half the  $k_f$  value for 4-dimethylaminoazobenzene. This can be attributed to the difference in basicity of the two substituents. The  $\text{p}K_a$  value for the conjugate acid of 4-dimethylaminoazobenzene in aqueous solution at 25°C is 3.5,<sup>38</sup> whereas the conjugate acid of 4-phenylazoaniline has a  $\text{p}K_a$  value of 2.76.<sup>38</sup> The strongly electron-withdrawing sulfonic



**Fig. 9.** Voltammograms of four monoazo dyes, 0.1 M acetate buffer, pH 4.6. (A) 7  $\mu$ M 4-dimethylaminoazobenzene,  $t_c = 40$  s; (B) 5  $\mu$ M 4-phenylazoaniline,  $t_c = 20$  s; (C) 10  $\mu$ M Methyl Orange,  $t_c = 10$  s; (D) 5  $\mu$ M 4-amino-4'-dimethylaminoazobenzene,  $t_c = 10$  s.



group reduces the  $k_f$  of Methyl Orange by a factor of seven in comparison with that of 4-dimethylaminoazobenzene.

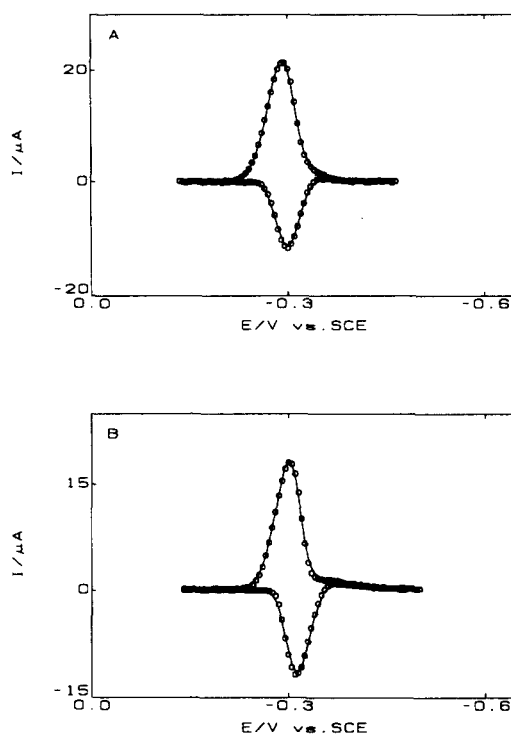


**Fig 10.** Observed and calculated voltammograms of Fig. 9A and B. (○) Experimental; (—) calculated for reaction scheme 2: (A)  $7\ \mu\text{M}$  4-dimethylaminoazobenzene,  $R = 0.9993$ ,  $s_y = 0.21\ \mu\text{A}$ ;  $s/s_y = 159$ ; (B)  $5\ \mu\text{M}$  4-phenylazoaniline,  $R = 0.9990$ ,  $s_y = 0.22\ \mu\text{A}$ ;  $s/s_y = 132$ .

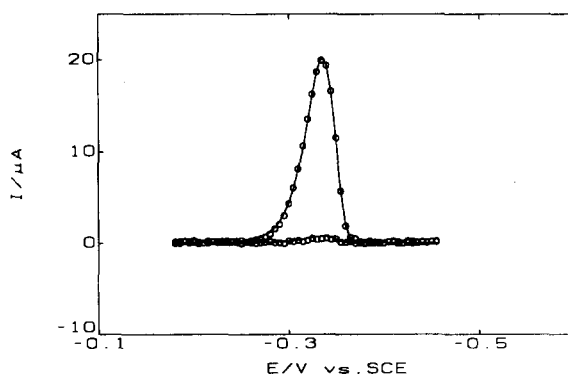


**Fig. 11.** Observed and calculated voltammograms of Fig 9D. (○) Experimental, (—) calculated for the four-electron one-step irreversible reduction model,  $R = 0.9995$ ,  $s_y = 0.14\ \mu\text{A}$ ;  $s/s_y = 140$ .

**TABLE 2**  
Kinetic and Thermodynamic Parameters at pH 4.6<sup>a</sup>

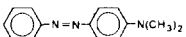
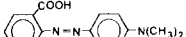
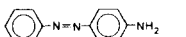
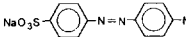
	$E^0/(V \text{ vs } SCE)$	$\alpha_1$	$k^0 (s^{-1})$	$\alpha_2$	$k_f (s^{-1})$	$R$	$s_y (\mu A)$	$s/s_y$
	-0.299	0.52	259	0.05	49.1	0.9993	0.21	159
	-0.251	0.49	225	0.12	42.2	0.9993	0.28	149
	-0.311	0.56	199	0.01	20.9	0.9990	0.21	132
	-0.288	0.51	204	0.03	6.8	0.9990	0.41	125

Figure 12 provides a comparison of the voltammogram of azobenzene with those of three monoazo dyes having a methoxy or hydroxy substituent. The voltammograms of the latter three dyes display two peaks, as in the case of azobenzene, due to the weak electron-donating methoxy and hydroxy substituents. The peak separations for the four dyes are different, however. This is explained by the different base strengths of the azo group of these compounds. The  $pK_a$  values for azobenzene, 4-methoxyazobenzene, 4-phenylazophenol in 20% ethanol–80%  $H_2SO_4$  at 25°C are -2.90, -1.36, and -1.02, respectively.<sup>38</sup> The smallest peak separation is seen with 2,2'-dihydroxyazobenzene due to the effect of the two hydroxy groups.

If the surface reaction mechanism of these four dyes were a two-step reduction, the first peaks would be a two-electron quasi-reversible reduction, and the second irreversible peaks would shift positively faster than the first quasi-reversible peaks and overlap the first peaks as the pH value of the solution decreases, as long as the peak potential difference between the two peaks is small enough. Figure 13A shows that the first peak of the voltammogram in Fig. 12D is well described by the two-electron quasi-reversible reduction model. Though a four-electron two-step reduction mechanism can fit the first peak, the first step current calculated is exactly the same as the total current and the second step current is zero, as shown in Fig. 13B. The same is true for the other three dyes.

Figure 13C presents a voltammogram of 2,2'-dihydroxyazobenzene at pH 1.80. It shows that the second peak has partially overlapped the first peak. The two-step model describes the partially overlapped peak well, as shown in Fig. 13D. We expect that at even lower pH values, the second peak would completely overlap the first peak, as in the case of Methyl Red. However, the first peak is shifted positive of 0 V, where the oxidation of the mercury electrode occurs.

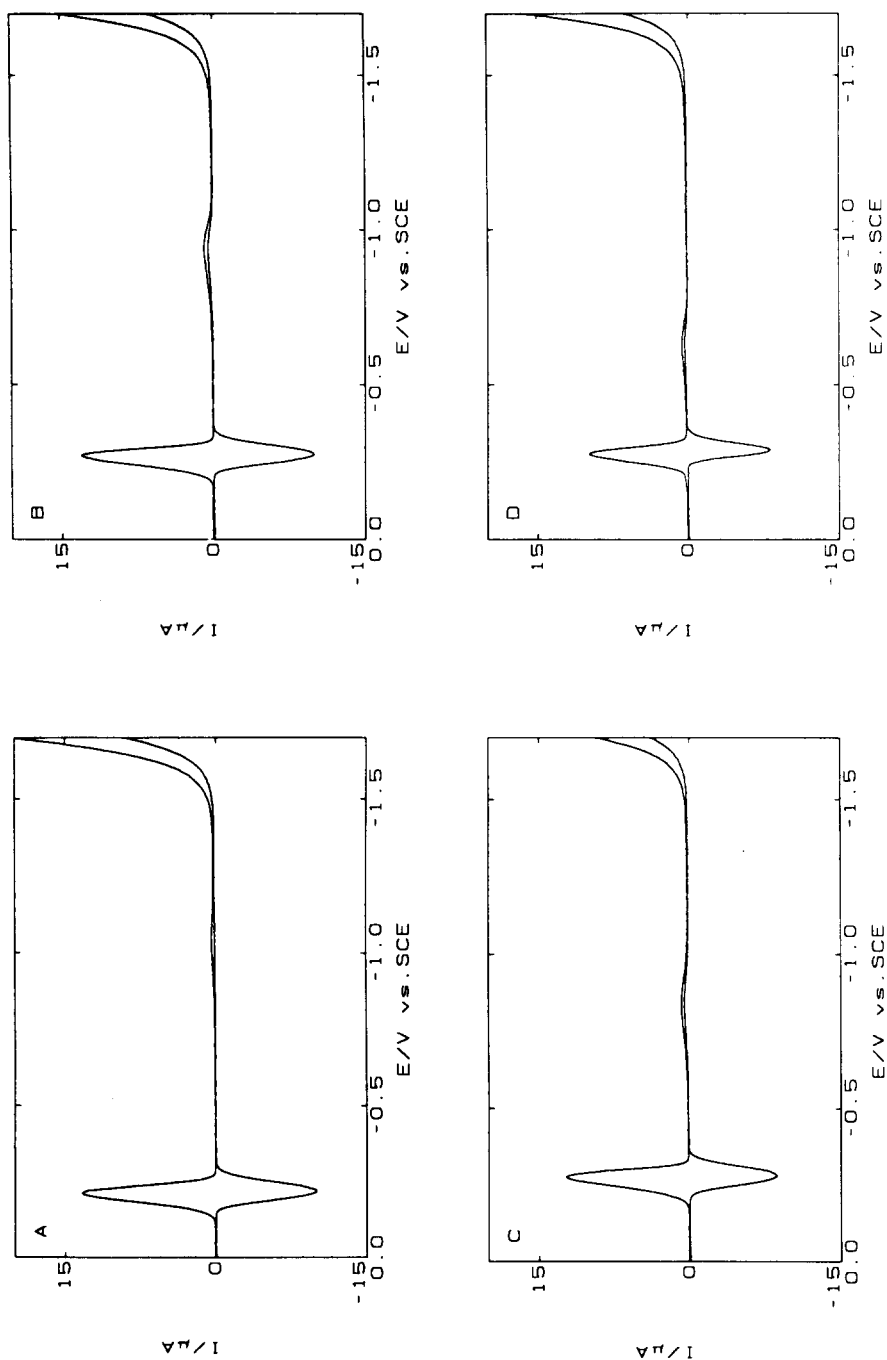
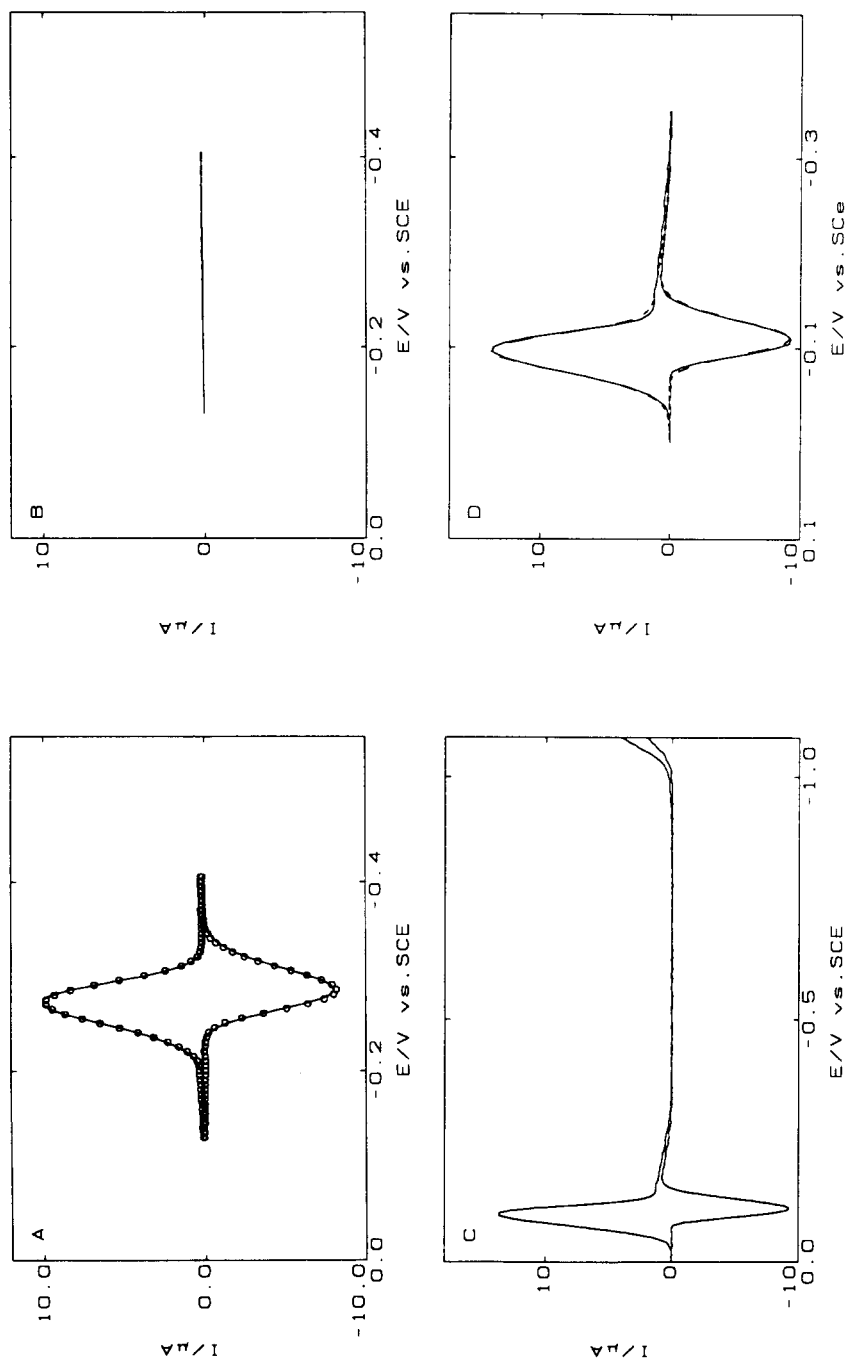


Fig. 12. Voltammograms of four monoazo dyes, 0.1 M acetate buffer, pH 4.6,  $f = 200$  Hz. (A) 10  $\mu$ M azobenzene,  $t_c = 5$  s; (B) 10  $\mu$ M 4-methoxyazobenzene,  $t_c = 5$  s; (C) 10  $\mu$ M 4-phenylazophenol,  $t_c = 5$  s; (D) 5  $\mu$ M 2,2'-dihydroxyazobenzene,  $t_c = 10$  s.



**Fig. 13.** (A) Observed and calculated currents of the first peak in Fig. 12D, (○) Experimental, (—) calculated for a two-electron quasi-reversible reduction mechanism,  $R = 0.9995$ ,  $s_y = 0.10 \mu\text{A}$ ,  $s/s_y = 173$ . (B) Calculated second step current for a two-step model. (C)  $5 \mu\text{M}$  2,2'-dihydroazobenzene in  $0.1 \text{ M}$  Britton-Robinson buffer,  $\text{pH } 1.8$ ,  $f = 200 \text{ Hz}$ ,  $t_c = 40 \text{ s}$ . (D) Observed and calculated currents of (C). (—) Experimental, (---) theoretical for reaction scheme 2,  $R = 0.9990$ ,  $s_y = 0.17 \mu\text{A}$ ,  $s/s_y = 138$ .

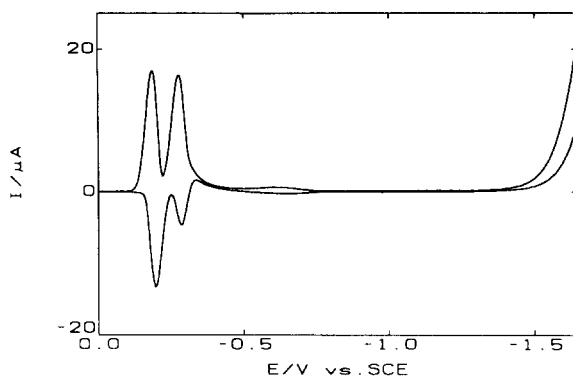
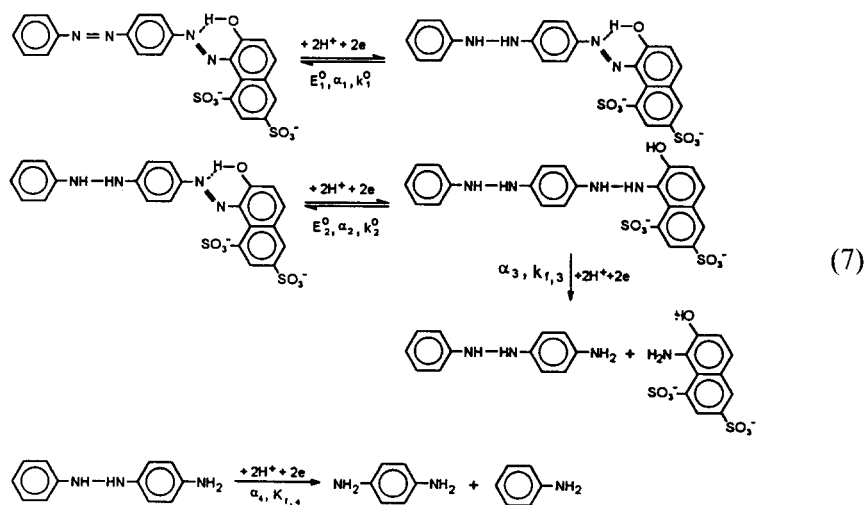


Fig. 14. Voltammogram of 10  $\mu\text{M}$  CI Acid Red 73, 0.1 M acetate buffer, pH 4.4,  $f = 200$  Hz.

From the results presented here, it may be expected that those monoazo dyes having strongly electron-donating substituents, such as amino, dimethylamino, or dihydroxy, would be biodegraded directly to amines anaerobically *in vivo*.

Having studied the kinetics of the model adsorbates for totally irreversible reduction (midazolam),<sup>32</sup> quasi-reversible reduction (azobenzene)<sup>33</sup> and quasi-reversible reduction followed by irreversible reduction (Methyl Red), we gain more understanding of the reduction of more complex disazo dyestuffs such as CI Acid Red 73 (C. I. 27290). Figure 14 shows a representative voltammogram of CI Acid Red 73 in 0.1 M acetate buffer at pH 4.4, in which three peaks are seen. The first peak is just like the first peak of azobenzene. The second peak is the Methyl Red type, corresponding to a four-electron two-step reduction, and the third peak is totally irreversible. These patterns suggest a mechanism such as:



The results of these studies can be used, then, to form reasonable hypotheses regarding the behavior of quite complex azo compounds. Furthermore, all of the compounds we have examined display the analytically attractive characteristic behavior of Figs 2 and 3. Thus, they are all accessible to determination by means of adsorptive square wave stripping voltammetry. In the absence of the COOL algorithm, the analysis can be quantified by comparison of net peak height with that of a standard. However, the availability of COOL provides the additional possibility of determining the surface concentration directly from the slope of the regression.

### ACKNOWLEDGMENT

This work was supported in part by the U.S. National Science Foundation under grant number CHE9208987.

### REFERENCES

1. Spadaro, J. T., Isabelle, L. & Renganathan, V., *Environ. Sci. Technol.*, **28** (1994) 1389.
2. Miller, J. A. & Miller, E. C., *Adv. Cancer Res.*, **1** (1953) 339.
3. Carruthers, C., *Anal. Chim. Acta*, **86** (1976) 273.
4. International Agency for Research on Cancer, *Some Aromatic Compounds, IARC Monogr. Eval. Carcinog. Risk Chem. Man*, Vol. 8. International Agency for Research on Cancer, Lyon, 1975, p.53.
5. Johnson, R. K. & Lichlenberger, F. J., *Developments Food Colours*, ed. J. Walford. Applied Science, London, 1980, Vol. 2, p. 114.
6. Marmion, D. M., *Handbook of U.S. Colorants*. Wiley, New York, 1991, 3rd edn., p.23.
7. Chung, K. T., Fulk, G. E. & Egan, M., *Appl. Environ. Microbiol.*, **35** (1978) 558.
8. Roxon, J. J., Ryan, A. J. & Wright, S. E., *Food Cosmet. Toxicol.*, **4** (1966) 419.
9. Roxon, J. J., Ryan, A. J. & Wright, S. E., *Food Cosmet. Toxicol.*, **5** (1967) 645.
10. Scheline, R. R., Nygaard, R. T. & Lonberg, B., *Food Cosmet. Toxicol.*, **8** (1970) 55.
11. Meyer, U., Biodegradation of Synthetic Organic Colorants. In *Microbial Degradation of Xenobiotics and Recalcitrant Compounds*, FEMS Symposium No. 12, ed. T. Leisinger, R. Hutter, A. M. Cook & J. Nuesch. Academic Press, New York, 1981, p. 371.
12. Rafii, F., Franklin, W. & Cerniglia, C. E., *Appl. Environ. Microbiol.*, **6** (1990) 2146.
13. Chung, K. T. & Stevens, S. E. Jr., *Environ. Toxicol. Chem.*, **12** (1993) 2121.
14. Brown, D. & Laboureur, P., *Chemosphere*, **12** (1983) 397.
15. Urushigawa, Y. & Yonezawa, Y., *Bull. Environ. Contam. Toxicol.*, **17** (1977) 214.

16. Liu, J. & Liu, H., *Environ. Pollut.*, **75** (1992) 273.
17. Chung, K. T., Stevens, S. E. Jr. & Cerniglia, C. E., *CRC Crit. Rev. Microbiol.*, **18** (1992) 175.
18. Laitinen, H. A. & Kneip, T. J., *J. Am. Chem. Soc.*, **78** (1956) 736.
19. Florence, T. M., *Aust. J. Chem.*, **18** (1965) 609.
20. Florence, T. M., *J. Electroanal. Chem.*, **52** (1974) 115.
21. Barek, J., Pastor, T. J., Votavova, S. & Zima, J., *Collect. Czech. Chem. Commun.*, **52** (1987) 2149.
22. Barek, J., Savarino, P., Sluchlikova, L. & Zima, J., *Collect. Czech. Chem. Commun.*, **59** (1994) 2397.
23. Stradings, J. P. & Glezer, V. T., *Encyclopedia of Electrochemistry of the Elements: Organic Section*, ed. A. J. Bard. Marcel Dekker, New York, 1979, Vol. 13, pp. 178, 179.
24. Thomas, F. G. & Boto, K. G., *The Chemistry of the Hydrazo, Azo and Azoxy Groups*, ed. S. Patai. Wiley, New York, 1975, Part 1, pp. 470, 168.
25. Boto, K. G. & Thomas, F. G., *Aust. J. Chem.*, **23** (1970) 43.
26. Kastening, B., *Ber. Bunsen Ges. Chem.*, **68** (1964) 979.
27. Laviron, E. & Mugnier, Y., *J. Electroanal. Chem.*, **111** (1980) 337.
28. Barek, J., Kvapilova, H., Mejstrik V., Petira, O. & Zima, J., *Collect. Czech. Chem. Commun.*, **55** (1990) 2636.
29. Osteryoung, J. G. & O'Dea, J. J. In *Electroanalytical Chemistry*, ed. A. J. Bard. Marcel Dekker, New York, 1986, Vol. 14, pp. 209–308.
30. Osteryoung, J. G., *Acc. Chem. Res.*, **26** (1993) 77.
31. Xu, G., O'Dea, J. J., Mahoney, L. A. & Osteryoung, J. G., *Anal. Chem.*, **66** (1994) 808.
32. O'Dea, J. J., Osteryoung, J. G. & Lane, T., *J. Phys. Chem.*, **90** (1986) 2761.
33. O'Dea, J. J., Ribes, A. & Osteryoung, J. G., *J. Electroanal. Chem.*, **345** (1993) 287.
34. O'Dea, J. J. & Osteryoung, J. G., *Anal. Chem.*, **65** (1993) 3090.
35. Meites L., *Polarographic Techniques*. Wiley-Interscience, New York, 1965, 2nd edn, p. 145.
36. Moreiras, D. & Solans, J., *Cryst. Struct. Comm.*, **9** (1980) 921.
37. Soriaga, M. P., Wilson, P. H. & Hubbard, A. T., *J. Electroanal. Chem.*, **142** (1982) 317.
38. Krueger, P. J., *The Chemistry of the Hydrazo, Azo and Azoxy Groups*, ed. S. Patai. Wiley, New York, 1975, Part 1, p. 168.